Research article

George Duffett*, Ralph Wirth, Mathieu Rayer, Emiliano R. Martins and Thomas F. Krauss

Metal-insulator-metal nanoresonators – strongly confined modes for high surface sensitivity

https://doi.org/10.1515/nanoph-2020-0199
Received March 16, 2020; accepted April 19, 2020

Abstract: Photonic and plasmonic refractive index sensors are able to detect increasingly smaller refractive index changes and concentrations of clinically relevant substances. They typically exploit optical resonances and aim to maximise the field overlap with the analyte in order to achieve high sensitivity. Correspondingly, they operate on the basis of maximizing the bulk sensitivity, which favours spatially extended modes. We note that this strategy, counter-intuitively, is not necessarily suitable for detecting biomolecules and one should focus on the surface sensitivity instead. Here, we show that by confining light tightly in metal-insulator-metal (MIM) nanoresonators, the surface sensitivity is significantly *increased* despite a clear *decrease* in bulk sensitivity. In particular, we experimentally show the operation of third order MIM resonators which support both extended surface plasmon polariton (SPP) modes and localized MIM modes. We are able to demonstrate that the MIM mode has a sensitivity of 55 nm/RIU to a 10 nm layer, which is approximately twice as high as that of the SPP mode. Overall, our work emphasizes the importance of the surface sensitivity over the more commonly used bulk sensitivity and it shows a novel approach for improving it. These insights are highly relevant for the design of next generation optical biosensors.

Keywords: nanocavities; plasmonics; refractive index sensing; surface sensitivity.

***Corresponding author: George Duffett**, Department of Physics, University of York, Heslington, York, YO10 5DD, UK, E-mail: george.duffett@york.ac.uk. https://orcid.org/0000-0001-7044-0982
Ralph Wirth and Mathieu Rayer: Osram Opto Semiconductors, Regensburg, Bayern, Germany
Emiliano R. Martins: University of Sao Paulo Sao Carlos School of Engineering, São Carlos, São Paulo, Brazil
Thomas F. Krauss: Department of Physics, University of York, York, UK

1 Introduction

Biosensors have applications in detecting and measuring pollutants, monitoring food quality, early disease detection and drug discovery [1]. The majority of optical biosensors use fluorescence methods, which provide excellent signal-to-noise ratio but are mainly confined to the laboratory setting [2, 3]. Label-free methods are intrinsically simpler and more suited for point-of-care or in-field applications. Label-free methods typically rely on photonic resonances to enhance the sensitivity. The light confined to the resonance is sensitive to its surroundings via the evanescent field of the resonant mode which overlaps with the media on the sensor surface [4]. When the media on the sensor surface experiences changes in refractive index, the resonance condition changes and the peak wavelength of the spectrum shifts, which is detected. The sensor surface can be functionalized such that only specific biological molecules can bind to the surface.

Many photonic and plasmonic biosensors have already been presented in the literature. The classical surface plasmon resonance (SPR) method has a high bulk sensitivity of 2500 nm/RIU [5, 6] and has been commercialized as the Biacore system for studying DNA, proteins, cells and viruses [7]. Classical SPR requires coupling light via a prism and careful control of the input angle. Localized surface plasmon resonance, e. g. using gold nanoparticles, relaxes the coupling requirement but compromises the sensitivity down to 500 nm/RIU [8]. A related option is to excite an SPR by patterning the metallic layer, a strategy that can reach a sensitivity of 700 nm/RIU [9] for gold nanohole arrays. Using periodic nanostructures also allows designing them such that they can operate without the need for a spectrometer, i. e. by spatially encoding spectral information [10, 11] or by monitoring the intensity of the transmitted signal [12].

The overlap of the resonant mode with the analyte and related changes provides the sensing information. Based on this understanding, an obvious consequence is to use extended modes that carry the majority of their field in the analyte. Surface plasmon modes are an ideal example for this strategy. Being modes that are bound to the interface

between the metal and the analyte, the majority of their electric field does indeed overlap with the analyte, resulting in their high sensitivity. Unfortunately, the sensitivity that is usually quoted is the "bulk" sensitivity [13–15], i. e. the sensitivity to refractive index changes in the bulk of the analyte, mainly because it is easy to measure. Many authors then implicitly assume that the bulk sensitivity is proportional to the surface sensitivity; for example, Homola et al. [6] state that "This suggests that the surface refractive index sensitivity is proportional to the bulk refractive index sensitivity … ". Here, we show that this extrapolation does not generally hold. Instead, we highlight that a higher surface sensitivity can be achieved with tightly confined modes in the same structure, even though their bulk sensitivity is much lower.

We use the metal-insulator-metal (MIM) geometry as an alternative sensing modality to illustrate this strategy. Remarkably, our MIM structure supports both confined and extended modes, which allows for a direct comparison. The MIM geometry is a textbook plasmonic system [16] and has already been studied in a variety of contexts [17]. For example, Baumberg et al. have studied the coupling between waveguide and antenna modes supported by the nanoparticle system [18] and have enhanced light emission [19]. Mikkelsen et al. have explored MIM modes in the context of controlling radiative processes [20, 21] and have used the MIM geometry to enhance the electric field and amplify third harmonic generation [22]. MIM structures have also been used for bulk refractive index sensing [14, 23] and as thermal emitters for optical gas sensing [24]. Their remarkably high surface sensitivity remains unexplored, however, which is the focus of this work, and we show values of 55 nm/RIU for a mode confined to a 10 nm thick dielectric layer, which is twice the surface sensitivity of the extended surface plasmon resonance in the same system.

2 Design

Our design is inspired by Lalanne et al. who recognized that MIM resonators can support modes of high effective index and low group velocity [25]. Such modes are tightly confined such that their evanescent tail is short and strongly overlaps with surface-bound biomolecules.

The operation of the MIM resonator (dip 2 in Figure 1b) can then be understood using a Fabry–Perot model [25, 26], in which the slow gap plasmon is reflected at either end of the top metal feature. The three layers forming the MIM are an optically thick gold layer on the bottom, an SiO_2 insulating layer and the gold island on top, which defines the resonator. The SiO_2 layer is formed as a continuous film which simplifies fabrication and reduces surface roughness. The choice of a continuous insulator layer as opposed to a discrete insulator layer has little impact on the confinement properties of the resonator. The field distribution shown in Figure 1c–e were simulated using a 3D finite element code (COMSOL®) using rounded corners to more accurately represent the fabricated resonators shown in Figure 2b. We note the strong spatial confinement of the E field to the resonator and hotspots at the edges of the top metal/dielectric interface for the MIM mode in Figure 1d.

3 Materials and methods

Our fabrication process is shown schematically in Figure 2a. The base plane is fabricated by template stripping [27] using 150 nm of gold deposited by electron beam evaporation onto an atomically flat silicon wafer. We found that template stripping provided a much smoother gold surface than direct evaporation onto the substrate. The 20 nm thick SiO_2 insulator layer is deposited using a bespoke pulsed-DC magnetron sputterer (100 W, 2.9 µS, 120 kHz, gas flow 17.5 sccm Ar, 10 sccm O_2). To define the resonator, we pattern a single PMMA layer (50 keV Raith Voyager, dose 300 µC/cm^2), evaporate 20 nm of gold (MBraun electron-beam evaporator) and lift-off the PMMA. Figure 2b shows an overview and a detail SEM micrograph of the fabricated structures.

4 Results and discussion

Figure 3a shows the mode spectrum of the resonators, measured by illuminating the array of Figure 2b with the collimated beam of a halogen lightbulb through a monochromator. We note three spectral features, i. e. dips around 630, 730 and 850 nm. We identify the 630 and 850 nm dips as extended SPR modes (Figure 1). From the COMSOL® model, we note that the optical field is not confined to the resonator in both cases and also that their spectral position depends on period. In contrast, the field distribution of the 730 nm feature is strongly confined to the metal nanostructure and the spectral position of the mode is independent of period. This MIM mode has an effective index of approximately 3, which we calculate by applying a simple Fabry Perot model to the resonator or by using MIM dispersion relations [16, 26]. We note that [25] predicts effective index values around $n_{\mathrm{eff}} = 7$ for a 20 nm thick dielectric layer by using a value $n = 3.5$ for the insulator, while we use SiO_2 with $n = 1.45$; the ratio in effective index can therefore be explained by the ratio of the refractive indices of the insulator material.

We first measure the bulk sensitivity (Figure 3a,b), then the surface sensitivity (Figure 3d,e). The bulk sensitivity is determined by applying DI water with varying salt concentrations to the surface and fitting Lorentzian

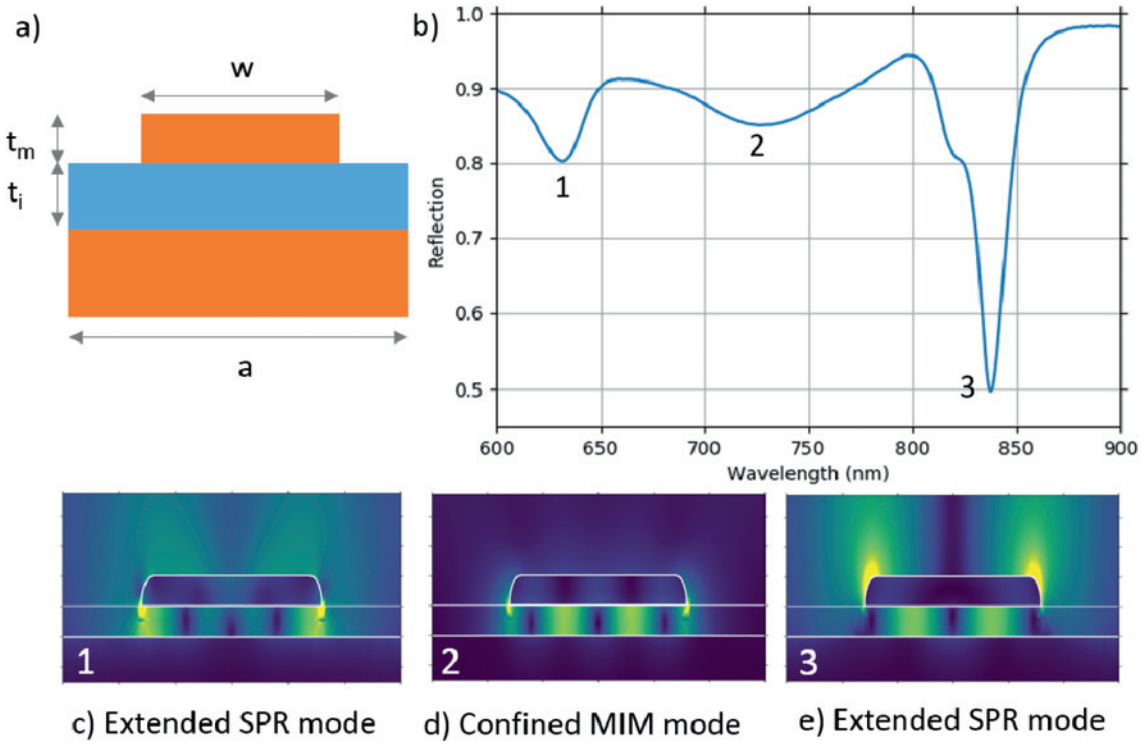

Figure 1: (a) Schematic of the structure showing top metal thickness, t_m, insulator thickness t_i resonator width, w, and period. (a, b) Spectrum and identification the various modes supported by the structure. (d) Plot of the electric field of the confined MIM mode. E field plots (c) and (e) are of the SPR modes at 640 and 840 nm respectively.

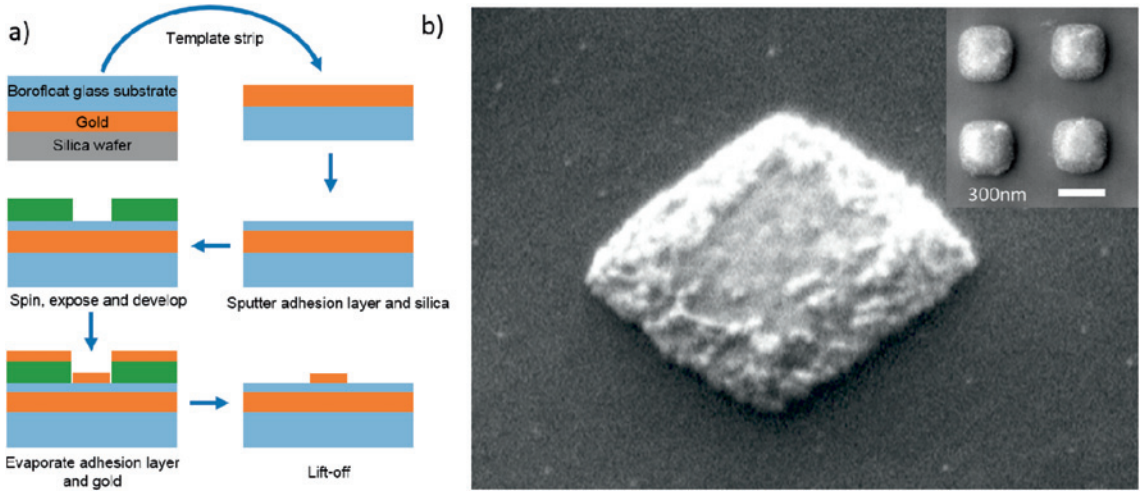

Figure 2: Fabrication of the MIM resonators. (a) Schematic of the fabrication process showing key steps. Adhesion layers are omitted for clarity. (b) SEM micrographs of the fabricated structures of 300 nm size.

functions to dips in the spectra (Figure 3a). We measure 540 nm/RIU sensitivity for dip 3, the extended SPR mode at 850 nm wavelength, which is close to the expected value of 500–700 nm/RIU [8, 9]. The MIM mode (dip 2), on the other hand, only shows 60 nm/RIU sensitivity in this measurement, which appears disappointing.

When it comes to surface sensitivity, however, the strong confinement of the MIM mode turns into a real advantage. We measured the surface sensitivity by sputtering a 10 nm silica layer onto the resonator surface and comparing the peak wavelength from the Lorentzian curve fit before and after sputtering. The MIM mode overlap with the

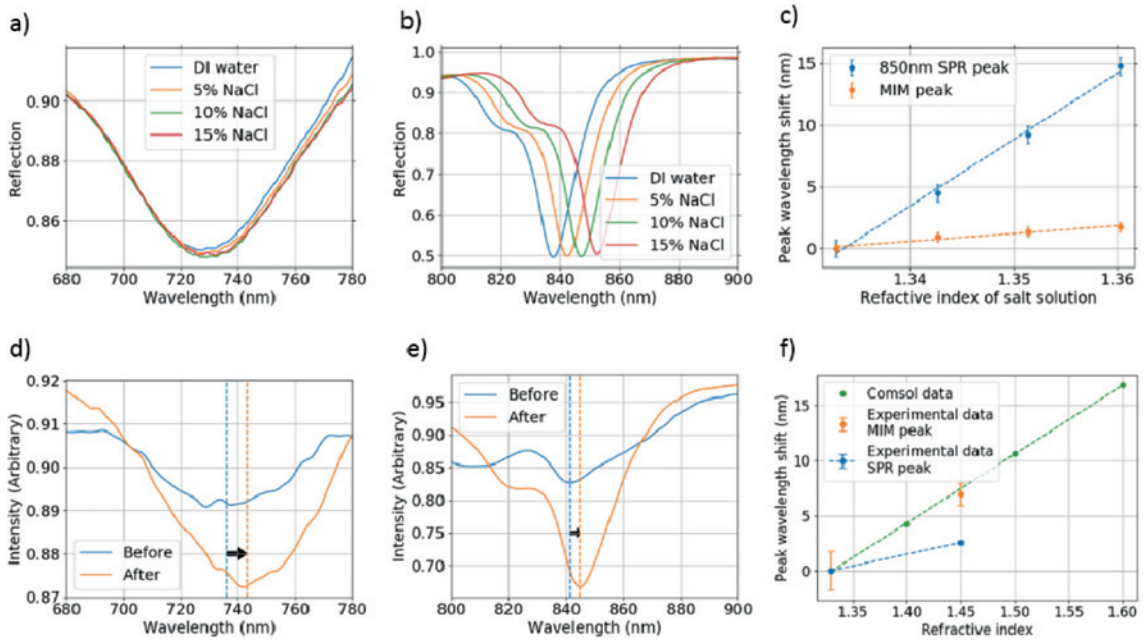

Figure 3: Sensitivity results comparing dips 2 and 3, i. e. the confined MIM and extended SPP mode, respectively. (a) MIM and (b) SPP bulk sensitivity spectra and (c) bulk peak wavelength shifts. (d) MIM and (e) SPP surface sensitivity spectra, before and after depositing 10 nm of silica onto the resonator. (f) Comparison of simulated surface sensitivity and experimental surface sensitivity in terms of wavelength shift.

10 nm layer is very large due to its strong confinement, so essentially all of the evanescent field overlaps with the 10 nm layer. This large mode overlap causes a peak wavelength shift of 7 nm. Taking the RI of DI water as 1.33 and sputtered silica as 1.45, the RI change is 0.12, which yields a surface sensitivity of 55 nm/RIU. By contrast, the extended SPR has a much lower overlap with the 10 nm layer since it extends much further into the analyte layer, resulting in a surface sensitivity of only 25 nm/RIU. This measured value is comparable to the value of 31 nm/RIU for a plasmonic nanohole array which we determine from the data shown in ref. [28].

We use the COMSOL model to better understand the origin of the high surface sensitivity. We place blocks of silica into various places, i. e. a) onto the top of the entire surface, b) only onto the top gold feature and c) only onto the side of the gold feature. We note that the simulated surface sensitivity for a) of 59 nm/RIU is in good agreement with the experiment (55 nm/RIU). The MIM also retains its high surface sensitivity when only the gold surface is coated with silica (Figure 4b), mimicking the case where the gold surface would be functionalized using standard procedures [29]. The fact that the surface sensitivity stays high in Figure 4c

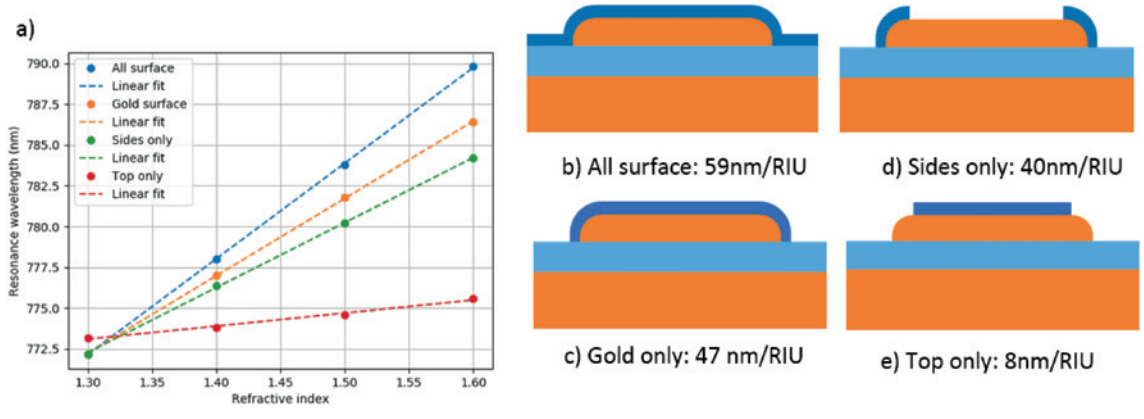

Figure 4: Comsol modelling highlighting the source of the MIM peak surface sensitivity. (a) Wavelength shifts resulting from coating different areas of the sensor surface (b–e). Covering only the edges of the resonator as in (d) results in much larger wavelength shifts than only covering the edges as in (e). Covering only the top surface as in (e) further highlights that the edges are the most sensitive part of the structure

highlights the fact that the majority of the sensitivity derives from the field overlap at the edges of the resonator. The field overlap between the MIM mode and the analyte, here represented by the thin film, can be determined as follows [30],

$$\mathrm{OI} = \frac{\int_{V_{\mathrm{Analyte}}} \epsilon(\mathbf{r},\omega)\tilde{\mathbf{E}}(\mathbf{r})\cdot\tilde{\mathbf{E}}(\mathbf{r})\mathrm{d}^3\mathbf{r}}{\int_{V_{\mathrm{Total}}} \tilde{\mathbf{E}}(\mathbf{r})\cdot\frac{\partial[\omega\epsilon(\mathbf{r},\omega)]}{\partial\omega}\tilde{\mathbf{E}}(\mathbf{r})\mathrm{d}^3\mathbf{r}}$$

where the overlap integral OI is the resonant electric field's overlap with the analyte volume (V_{analyte}) on the sensor surface, normalized by the electric field on resonance integrated over all space (V_{total}) The electric field normalisation is described in more detail in refs [31, 32].

In order to verify that the mode overlap is the key quantity to explain these results, we calculate the overlap integrals between the respective modes and the analyte. For the case of full surface coverage (Figure 4a), we find that 9% of the MIM E-field overlaps with the analyte on the sensor surface, as opposed to 6% for the surface plasmon mode. This 1.5× ratio corresponds reasonably well to the ratio (55 nm/RIU vs. 25 nm/RIU) observed experimentally.

5 Conclusions

We have shown that metal-insulator metal (MIM) modes have a significantly higher surface sensitivity than other sensing modalities based on the tight confinement they offer. We note that surface sensitivity is the key figure of merit for biomolecular applications because surface-bound molecules are typically located within 5–10 nm of the sensor surface. Importantly, we show that surface sensitivity is not directly related to bulk sensitivity, which is the quantity usually measured. In particular, we show a surface sensitivity of 55 nm/RIU for the particular MIM mode considered here while we only measure 25 nm/RIU for the SPR mode in the same structure. Conversely, the SPR mode exhibits a bulk sensitivity of 540 nm/RIU, while the MIM mode only shows 60 nm/RIU.

We believe that a number of further improvements are possible. The effective index of the MIM mode studied here broadly agrees with the model of [25], but the depth of the resonance does not. This suggests that deeper and sharper resonances are possible that can e. g. be achieved by improving the surface roughness of the resonator. Secondly, reducing the size of the resonator down to that of the first order mode will increase the mode overlap with the analyte and further increase the surface sensitivity. The first order mode would require resonator sizes of order 70–80 nm for the same wavelength window, which is realistic but more difficult to realise reproducibly. Preliminary simulations suggest that surface sensitivities in excess of 100 nm/RIU for a 10 nm layer may be possible, which is a very exciting prospect.

Overall, it is clear that increasing the surface sensitivity allows us to detect more binding events to a functionalized surface, in turn leading to lower limits of detection. We trust that the discussion of surface vs. bulk sensitivity and the demonstration of high sensitivity MIM resonators will inform the design and evaluation of the next generation of biosensors.

Acknowledgements: We would like to thank Dr. Christopher Reardon (University of York) for technical assistance with the SEM and Augusto Martins (University of São Paulo) for fruitful simulation discussions. The authors acknowledge financial support by the EPSRC of the UK (Grants EP/P02324X/1 and EP/P030017/1). Prof. Thomas F. Krauss acknowledges a Royal Society Wolfson Merit Award.

References

[1] P. Mehrotra, "Biosensors and their applications – a review," *J. Oral Biol. Craniofacial Res.*, vol. 6, no. 2, pp. 153–159, 2016.
[2] M. Bauch, K. Toma, M. Toma, Q. Zhang, and J. Dostalek, "Plasmon-enhanced fluorescence biosensors: a review," *Plasmonics*, vol. 9, no. 4, pp. 781–799, 2014.
[3] C. R. Taitt, G. P. Anderson, and F. S. Ligler, "Evanescent wave fluorescence biosensors: advances of the last decade," *Biosens. Bioelectron.*, vol. 76, pp. 103–112, 2016.
[4] G. Pitruzzello, and T. F. Krauss, "Photonic crystal resonances for sensing and imaging," *J. Opt.*, vol. 20, no. 7, Art no. 073004, 2018.
[5] J. Homola, "Present and future of surface plasmon resonance biosensors," *Anal. Bioanal. Chem.*, vol. 377, no. 3, pp. 528–539, 2003.
[6] J. Homola, "Surface plasmon resonance sensors for detection of chemical and biological species," *Chem. Rev.*, vol. 108, no. 2. pp. 462–493, 2008.
[7] GE, "SPR systems," *Gen. Electric Life Sci.*, 2018. Available at: https://www.gelifesciences.com/en/gb/solutions/protein-research/products-and-technologies/spr-systems [accessed: Dec. 12, 2019].
[8] M.-C. Estevez, M. A. Otte, B. Sepulveda, and L. M. Lechuga, "Trends and challenges of refractometric nanoplasmonic biosensors: a review," *Anal. Chim. Acta*, vol. 806, pp. 55–73, 2014.
[9] X. Li, M. Soler, C. I. Özdemir, A. Belushkin, F. Yesilköy, and H. Altug, "Plasmonic nanohole array biosensor for label-free and real-time analysis of live cell secretion," *Lab Chip*, vol. 17, no. 13, pp. 2208–2217, 2017.
[10] G. J. Triggs, Y. Wang, C. P. Reardon, M. Fischer, G. J. O. Evans, and T. F. Krauss, "Chirped guided-mode resonance biosensor," *Optica*, vol. 4, no. 2, Art no. 229, 2017.

[11] F. Yesilkoy, E. R. Arvelo, Y. Jahani, and M. Liu, "Ultrasensitive hyperspectral imaging and biodetection enabled by dielectric metasurfaces," *Nat. Photonics*, vol. 13, no. 6, pp. 390–396, 2019.
[12] A. E. Cetin, A. F. Coskun, B. C. Galarreta, and M.Huang, "Handheld high-throughput plasmonic biosensor using computational on-chip imaging," *Light Sci. Appl.*, vol. 3, no. 1, Art no. e122, 2014.
[13] P. K. Sahoo, S. Sarkar, and J. Joseph, "High sensitivity guided-mode- resonance optical sensor employing phase detection," *Sci. Rep.*, vol. 7, pp. 7607, 2017.
[14] A. Cattoni, P. Ghenuch, A.-M. Hagiri-Gosnet, et al., "λ3/1000 plasmonic nanocavities for biosensing fabricated by soft UV nanoimprint lithography," *Nano Lett.*, vol. 11, no. 9, pp. 3557–3563, 2011.
[15] H. Chen, X. Kou, Z. Yang, W. Ni, and J. Wang, "Shape- and size-dependent refractive index sensitivity of gold nanoparticles," *Langmuir*, vol. 24, no. 10, pp. 5233–5237, 2008.
[16] S. A. Maier, *Plasmonics: Fundamentals and Applications*, New York, NY, Springer, 2007.
[17] C. Ciracì, R. T. Hill, J. J. Moick, et al., "Probing the ultimate limits of plasmonic enhancement," Science, vol. 337, no. 6098, pp. 1072–1074, 2012.
[18] R. Chikkaraddy, X. Zheng, F. Benz, et al., "How ultranarrow gap symmetries control plasmonic nanocavity modes: from cubes to spheres in the nanoparticle-on-mirror," *ACS Photonics*, vol. 4, no. 3, pp. 469–475, 2017.
[19] N. Kongsuwan, A. Demetriadou, R. Chikkaraddy, et al., "Suppressed quenching and strong-coupling of purcell-enhanced single-molecule emission in plasmonic nanocavities," *ACS Photonics*, vol. 5, no. 1, pp. 186–191, 2018.
[20] T. B. Hoang, G. M. Akselrod, and M. H. Mikkelsen, "Ultrafast room-temperature single photon emission from quantum dots coupled to plasmonic nanocavities," *ACS Nano Lett.*, vol. 16, pp. 270–275, 2015.
[21] A. Rose, T. B. Hoang, F. McGuire, et al., "Control of radiative processes using tunable plasmonic nanopatch antennas," *Nano Lett.*, vol. 14, no. 8, pp. 4797–4802, 2014.
[22] J. B. Lassiter, X. Chen, X. Liu, et al., "Third-harmonic generation enhancement by film-coupled plasmonic stripe resonators," *ACS Photonics*, vol. 1, no. 11, pp. 1212–1217, 2014.
[23] N. Liu, M. Mesch, T. Weiss, M. Hentschel, and H. Giessen, "Infrared perfect absorber and its application as plasmonic sensor," *Nano Lett.*, vol. 10, no. 7, pp. 2342–2348, 2010.
[24] A. Lochbaum, Y. Fedoryshyn, A. Dorodnyy, U. Koch, C. Hafner, and J. Leuthold, "On-chip narrowband thermal emitter for mid-IR optical gas sensing," *ACS Photonics*, vol. 4, no. 6, pp. 1371–1380, 2017.
[25] J. Yang, C. Sauvan, A. Jouanin, S. Collin, J.-L. Pelouard, and P. Lalanne, "Ultrasmall metal-insulator-metal nanoresonators: impact of slow-wave effects on the quality factor," *Opt. Express*, vol. 20, no. 15, pp. 16880–16891, 2012.
[26] N. Vogel, J. Zieleniecki, and I. Köper, "As flat as it gets: ultrasmooth surfaces from template-stripping procedures," *Nanoscale*, vol. 4, no. 13, p. 3820–3832, 2012.
[27] A. E. Cetin, D. Etezadi, B. C. Galarreta, M. P. Busson, Y. Eksioglu, and H. Altug, "Plasmonic nanohole arrays on a robust hybrid substrate for highly sensitive label-free biosensing," *ACS Photonics*, vol. 2, no. 8, pp. 1167–1174, 2015.
[28] M. Oliverio, S. Perotto, G. C. Messina, L. Lovato, and F. De Angelis, "Chemical functionalization of plasmonic surface biosensors: a tutorial review on issues, strategies, and costs," *ACS Appl. Mater. Interfaces*, vol. 9, no. 35, pp. 29394–29411, 2017.
[29] I. D. Block, N. Ganesh, M. Lu, and B. T. Cunningham, "A sensitivity model for predicting photonic crystal biosensor performance," *IEEE Sens. J.*, vol. 8, no. 3, pp. 274–280, 2008.
[30] S. I. Bozhevolnyi, T. Søndergaard, "General properties of slow-plasmon resonant nanostructures: nano-antennas and resonators," *Opt. Express*, vol. 15, no. 17, 2007.
[31] J. Yang, H. Giessen, P. Lalanne, "Simple Analytical Expression for the Peak-Frequency Shifts of Plasmonic Resonances for Sensing," *Nano Lett*, vol. 15, no. 5, pp. 439–444, 2015.
[32] P. Lalanne, W. Yan, K. Vynck, C. Sauvan, J. P Hugonin, "Light Interaction with Photonic and Plasmonic Resonances," *Laser & Photonics Reviews*, vol. 12, no. 5, 1700113, 2018.